Supplementary Information (SI) for Journal of Materials Chemistry A.

Supporting Information for

Plasma-assisted nitrogen-doped NiHf nanoalloy for efficient seawater electrolysis

Ran Ma,[a] Jianhua Meng,[a] Rui Chao,[a] Xiao Ma,[e] Lin Zhang,[e] Jikai Li,[a] Pengfei Guo,[a] Yan Jia,[a] Zhiyuan Jiang,[a] Guoxiu Wang,[b] Lu Liu,[, c] Xun Cui,[*, d] Yang Yang,[*, a] and Hao Tian[*, b]*

[a]Key Laboratory of Chemical Additives for China National Light Industry, College of Chemistry and Chemical Engineering, Shaanxi University of Science and Technology, Xi'an, 710021, China.

[b]Centre for Clean Energy Technology School of Mathematical and Physical Sciences, Faculty of Science University of Technology Sydney, NSW, 2007, Australia.

[c]Institute of Sustainability for Chemicals, Energy and Environment (ISCE^2), Agency for Science, Technology and Research (A*STAR), 1 Pesek Road, Jurong Island, Singapore 627833, Republic of Singapore.

[d]State Key Laboratory of New Textile Materials and Advanced Processing, Wuhan Textile University, Wuhan, 430200, China.

[e]State Key Laboratory of Solidification Processing, School of Materials Science and Engineering, Northwestern Polytechnical University, YouyiXi Road 127, Xi'an 710072, China.

Corresponding Authors

*E-mail: yyang399@sust.edu.cn (Yang Yang);

hao.tian@uts.edu.au (Hao Tian);

Liu_Lu@isce2.a-star.edu.sg (Lu Liu);

xcui@wtu.edu.cn (Xun Cui).

Contents

1. Experimental S3
   1.1. Chemicals and Materials S3
   1.2. Synthesis of Catalysts S3
      1.2.1. Treatment of nickel foam S3
      1.2.2. Preparation of Hf-doped β-$Ni(OH)_2$@NF S4
      1.2.3. Preparation of nanoalloy catalysts S4
   1.3. Materials Characterization S5
   1.4. Electrochemical Measurement S6
2. Additional Data and Figures S8
   Figure S1 .... S8
   Figure S2 .... S8
   Figure S3 .... S9
   Figure S4 .... S9
   Figure S5 .... S10
   Figure S6 .... S10
   Figure S7 .... S11
   Figure S8 .... S11
   Figure S9 .... S12
   Figure S10 .... S12
   Figure S11 .... S13
   Figure S12 .... S13
   Figure S13 .... S14
   Figure S14 .... S14
   Table S1 .... S15
   Table S2 .... S15
   Table S3 .... S16
   Table S4 .... S16
   Table S5 .... S17
   Table S6 .... S17
   Table S7 .... S18
Reference S19

1. Experimental

1.1 Chemicals and Materials

Nickel(II) nitrate hexahydrate ($Ni(NO_3)_2 \cdot 6H_2O$; 98%, CAS No.13478-00-7. Alfa Aesar), hafnium(IV) chloride ($HfCl_4$; 99.5%, CAS No.13499-05-3. Macklin), urea (CH_4N_2O; 99%, CAS No.57-13-6, Aladdin), potassium hydroxide (KOH; 90%, CAS No. 1310-58-3, Macklin), seawater (Xiamen, Fujian; Shandong, Qingdao; Liaoning, Huludao; Hainan), ethanol (C_2H_5OH; 98%, CAS No. 64-17-5, Sinopharm), platinocarbon (Pt/C; 20%, Sinopharm), and Nafion solution (5%, CAS No. 31175-20-9, Sigma-Aldrich) were analytical grade and used without further purification. Ultrapure water (⩾18.2 MΩ cm) was purified by an Ulupure UPR-III-10T (Sichuan YOUPU Ultrapure Technology Corporation) system. Nickel foam (NF, thickness ~1.5 mm) was purchased from Kunshan Lvchuang Electronic Technology Corporation.

1.2 Synthesis of Catalysts

1.2.1 Treatment of nickel foam

Nickel foam (NF) was treated using plasma etching technology. Specifically, both sides of the NF were exposed to Ar (99.999%) atmosphere at a radiofrequency power of 100 W and a chamber pressure of approximately 75 Pa for 5 minutes. Subsequently, the treated NF was ultrasonicated sequentially in hydrochloric acid, acetone, ethanol, and water for 10 minutes each. The surface was then dried using nitrogen gas and stored for further use.

1.2.2 Preparation of Hf-doped β-$Ni(OH)_2$@NF

Hf-doped β-$Ni(OH)_2$@NF (Hf-$Ni(OH)_2$@NF) was synthesized *via* a one-step hydrothermal method. First, 174.5 mg of $Ni(NO_3)_2 \cdot 6H_2O$ and 96.1 mg of $HfCl_4$ were dissolved in 20 mL of ultrapure water. After mixing thoroughly, 270.2 mg of urea was added, and the mixture was fully dissolved again. The resulting precursor solution was transferred into a hydrothermal reactor containing a piece of nickel foam (1×4 cm). The reactor was placed in an electrically heated drying oven and maintained at 120 °C for 6 h. After natural cooling to room temperature, the product was washed with water and ethanol and dried using nitrogen gas for subsequent use.

1.2.3 Preparation of nanoalloy catalysts

Synthesis of N-NiHf@NF: Hf-$Ni(OH)_2$@NF to synthesize N-doped NiHf@NF alloy by ammonia-Plasma. The sample was thermally treated in a 10% NH_3/Ar atmosphere with a heating rate of 5 °C min^{-1} until reaching 300 °C, where it was maintained for 20 min. Upon stabilization at the target temperature, the plasma was ignited by applying a radiofrequency (RF) power of 200 W under a dynamic chamber pressure of ~75 Pa. The system was allowed to cool naturally to ambient temperature, yielding the final N-NiHf@NF catalyst.

Synthesis of NiHf@NF: The Hf-$Ni(OH)_2$@NF precursor was subjected to plasma treatment in a 10% Ar/H_2 gas mixture. The temperature was first raised to 300°C at a heating rate of 5°C min^{-1} and maintained for 20 min. Upon reaching the target temperature, a RF power of 200 W was applied. The sample was allowed to cool naturally to room temperature, yielding the final NiHf@NF catalyst.

Synthesis of NiHf@NF(CVD): Using Hf-$Ni(OH)_2$@NF as the precursor, the chemical vapor deposition (CVD) method was adopted. The sample was heated to 600°C at a controlled rate of 5°C min^{-1} in a 10% Ar/H_2 atmosphere and maintained at this temperature for 1 hour to ensure complete reaction. After natural cooling to room temperature, the final product was obtained as a well-defined NiHf@NF(CVD).

1.3 Materials Characterization

X-ray diffraction (XRD) patterns were collected on a Bruker D8 Advance X-ray diffractometer (Germany) equipped with a Cu-Kα radiation source (λ = 1.5418 Å). The instrument operated at 40 kV and 40 mA. Data were collected over a 2θ range of 5° to 70° at a scanning rate of 5° min^{-1}. Scanning electron microscopy (SEM) was operated on a Thermo Scientific Apreo 2C scanning electron microscope at an accelerating voltage of 15 kV. High-resolution TEM, selected area electron diffraction (SAED) patterns, and high-angle annular dark-field-scanning transmission electron microscopy (HAADF-STEM) images and corresponding elemental mappings were recorded on a FEI Talos F200X instrument coupled four in-column silicon drift Super-X energy-dispersive X-ray spectroscopy (EDS) signal detectors at 200 kV.

X-ray absorption fine structure (XAFS) measurements were performed at the Singapore synchrotron radiation facility (SSRF) with an electron energy of 700 MeV and a magnetic field of 4.5 T. The synchrotron radiation used had a characteristic photon energy of 1.47

keV and a wavelength of 0.845 nm. All spectra were collected under identical environmental conditions. Athena and Artemis software packages[1]. X-ray photoelectron spectroscopy (XPS) was performed on a Thermo Fisher ESCALAB Xi+ X-ray photoelectron spectrometer with an Al Kα radiation source. All data were calibrated using the C 1s peak at 284.8 eV.

1.4. Electrochemical Measurement

The HER activity and performance evaluation: All electrochemical measurements were performed using a CHI 760E potentiostat with a standard three-electrode system. A carbon rod served as the counter electrode, while a Hg/HgO electrode (Gaoss Union, 1.0 M KOH) was employed as the reference electrode.

The fabrication of Pt/C@NF working electrodes: To prepare the Pt/C electrode for comparison, 5 mg of Pt/C and 20 μL of Nafion were dispersed in 600 μL of ethanol and 400 μL of deionized water in a small sealed tube. The mixture was sonicated for 30 min and then coated onto a NF substrate that was dried in air overnight.

The pH value of 1.0 M KOH electrolyte was determined to be 13.97 (standard deviation of three independent measurements) using a calibrated pH meter. All measured potentials *vs* Hg/HgO were converted to the reversible hydrogen electrode (RHE) scale according to the Nernst equation:

$$E_{RHE} = E_{Hg/HgO} + 0.0591 \times pH + 0.098$$

For 1 M KOH (pH 13.97), this yielded:

$$E_{RHE} = E_{Hg/HgO} + 0.921 \text{ V}$$

The corresponding conversion equations for different electrolyte systems were:

$E_{RHE} = E_{Hg/HgO} + 0.912$ V (1.0 M KOH + 0.5 M NaCl)

$E_{RHE} = E_{Hg/HgO} + 0.922$ V (Fujian seawater)

$E_{RHE} = E_{Hg/HgO} + 0.915$ V (Hainan seawater)

$E_{RHE} = E_{Hg/HgO} + 0.919$ V (Liaoning seawater)

$E_{RHE} = E_{Hg/HgO} + 0.919$ V (Shandong seawater)

Linear sweep voltammetry (LSV) was conducted from -0.7 to -1.5 V (*vs.* Hg/HgO) at a scan rate of 5 mV s^{-1}. The double-layer capacitance (C_{dl}) was determined through cyclic voltammetry in the non-Faradaic potential region (-0.8 to -0.7 V *vs.* Hg/HgO). Electrochemical impedance spectroscopy (EIS) measurements were carried out at -1.02 V (*vs.* Hg/HgO) over a frequency range of 200 kHz to 3 kHz with a 10 mV AC amplitude. All current densities were normalized to the geometric surface area of the working electrode that was in direct contact with the alkaline electrolyte.

Study of electrochemical corrosion resistance mechanism: The corrosion resistance of the materials was evaluated using potentiodynamic polarization (PDP) measurements and chronopotentiometric (E-t) analysis. PDP curves were constructed by determining Tafel plot parameters to obtain the corrosion potential (E_{corr}) and corrosion current density (j_{corr}) [2,3]. The polarization scans were performed over a potential range of 0.2 to -0.7 V (*vs.* Hg/HgO) with a scan rate of 5 mV s^{-1}. The electrochemical stability of the N-NiHf@NF electrode was assessed through chronopotentiometric testing at a constant current density of 100 mA cm^{-2} for 110 h. This extended stability test under high current conditions provided critical insights into the long-term durability of the catalyst in corrosive environments.

2. Additional Data and Figures

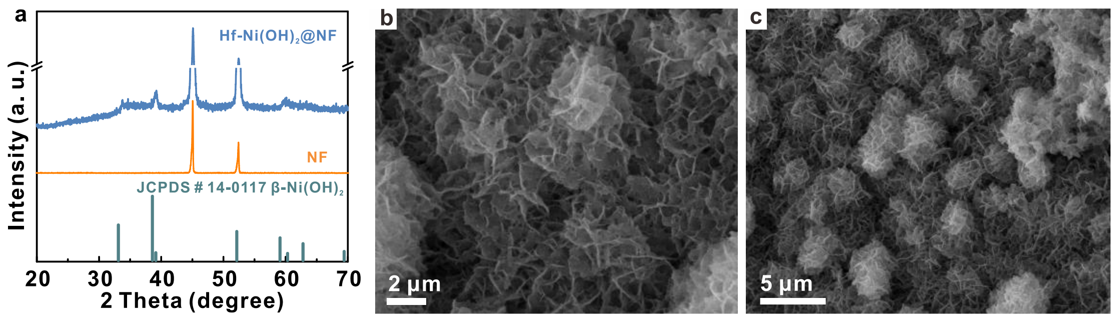

Figure S1. Physical characterization of Hf-Ni$(OH)_2$@NF. (a) XRD pattern, (b) SEM image with different magnification of (b) and (c).

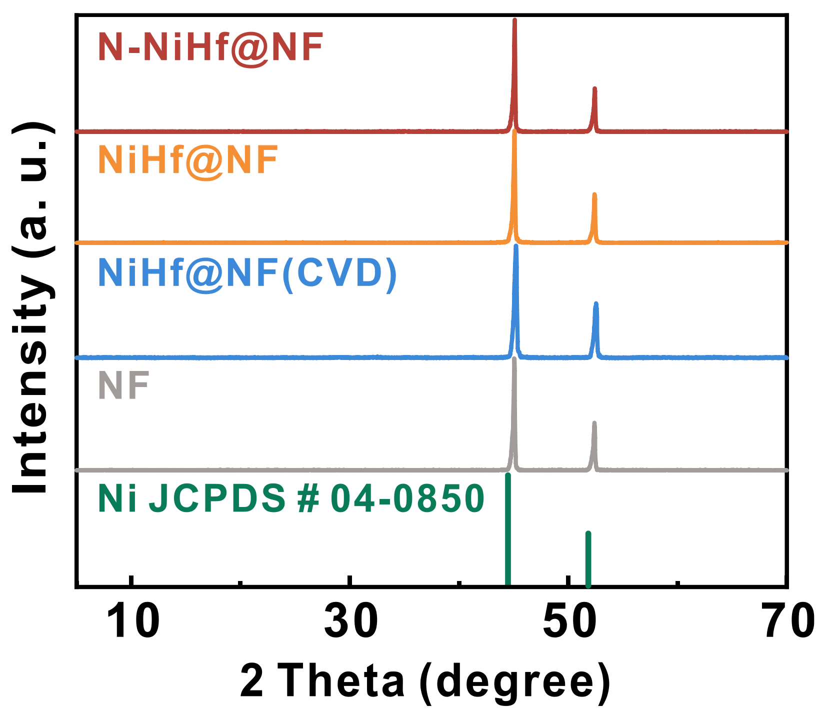

Figure S2. XRD patterns of as-prepared N-NiHf@NF, NiHf@NF, NiHf@NF(CVD) and NF.

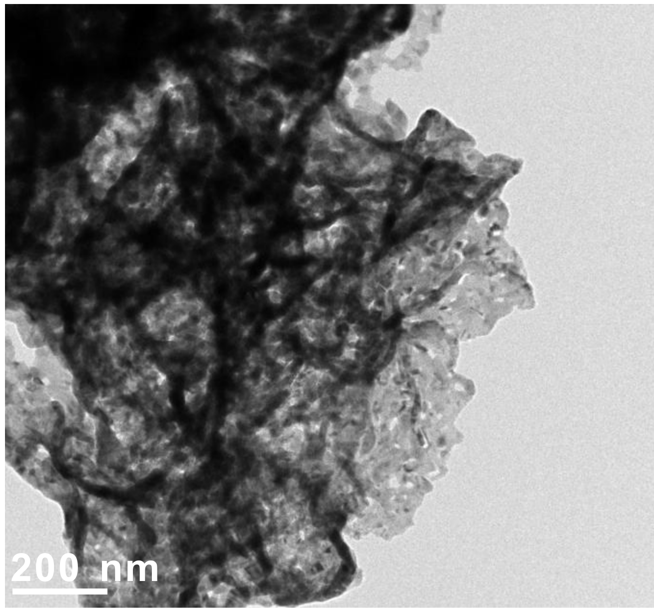

Figure S3. The TEM image of N-NiHf@NF.

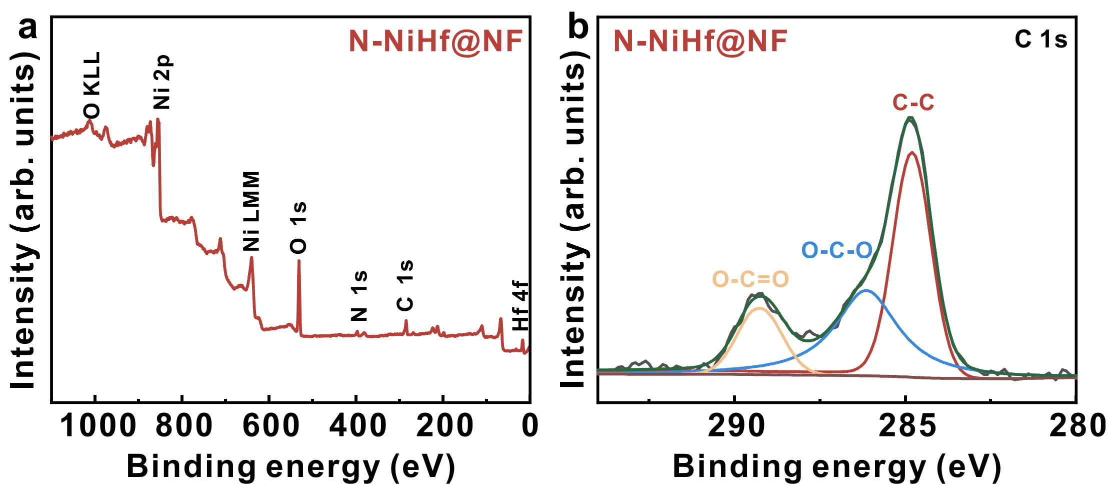

Figure S4. XPS analysis of N-NiHf@NF (a) Survey XPS, and (b) High-resolution C 1s spectra.

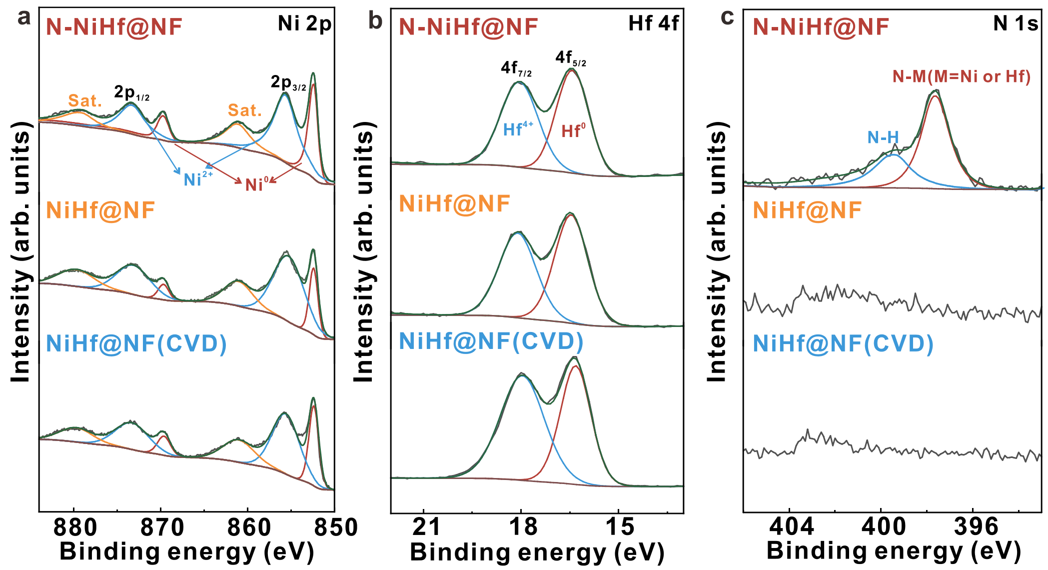

Figure S5. High-resolution XPS profiles for (a) Ni 2p, (b) Hf 4f, and (c) N 1s of three nanoalloys.

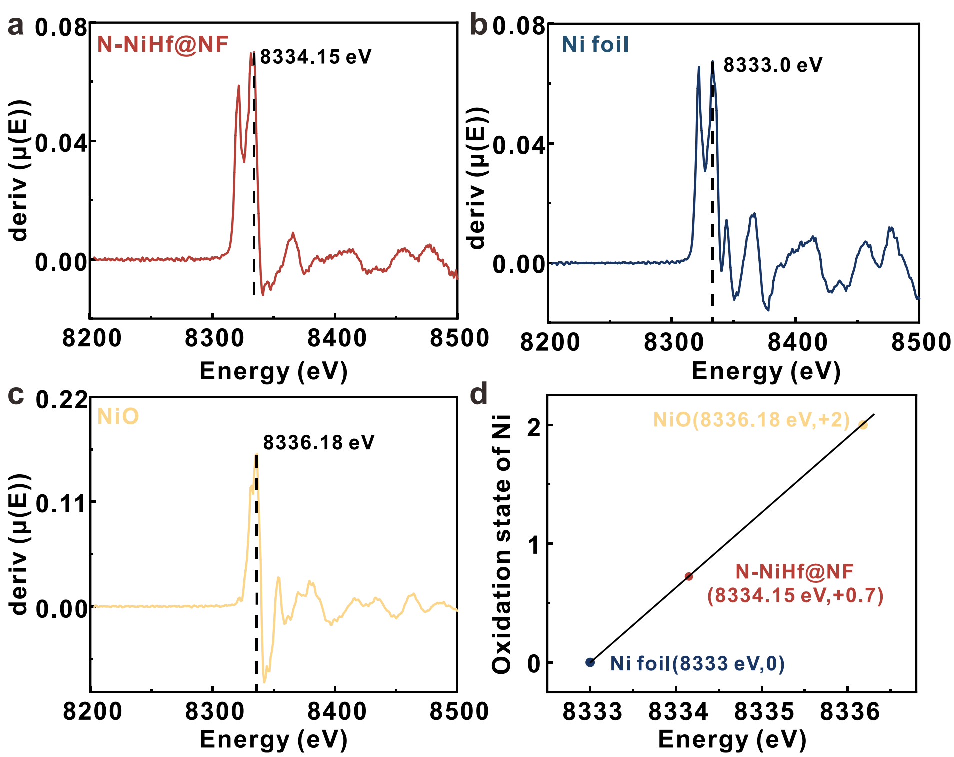

Figure S6. The first derivative curves of the XANES spectra of Ni K-edge for N-NiHf@NF and reference samples. (a) N-NiHf@NF, (b) Ni foil, (c) NiO, (d) Valence states of N-NiHf@NF(Ni) got from XANES spectra of Ni K-edge.

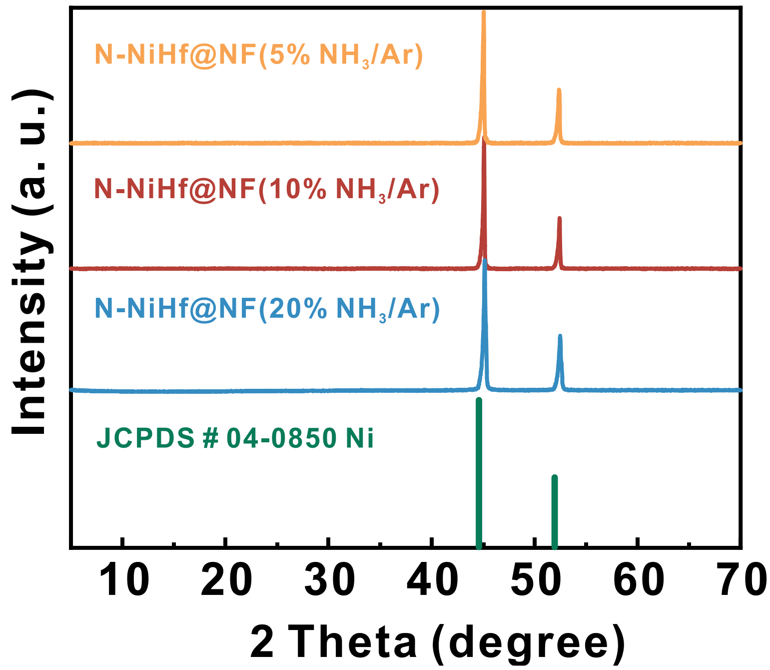

Figure S7. XRD patterns of N-NiHf@NF(5% NH_3/Ar), N-NiHf@NF(10% NH_3/Ar), and N-NiHf@NF(20% NH_3/Ar).

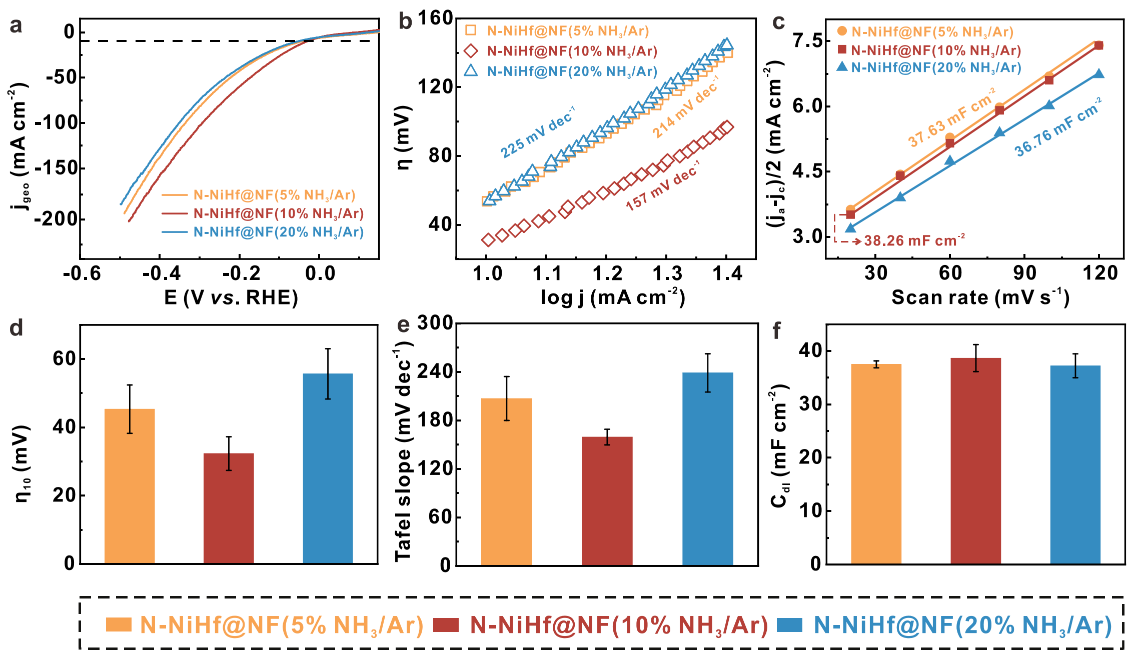

Figure S8. Electrochemical performance characterization results of N-NiHf@NF catalysts with different N contents: (a) LSV curves, (b) Tafel slope, (c) C_{dl}, (d-f) repeatability test data and error bar.

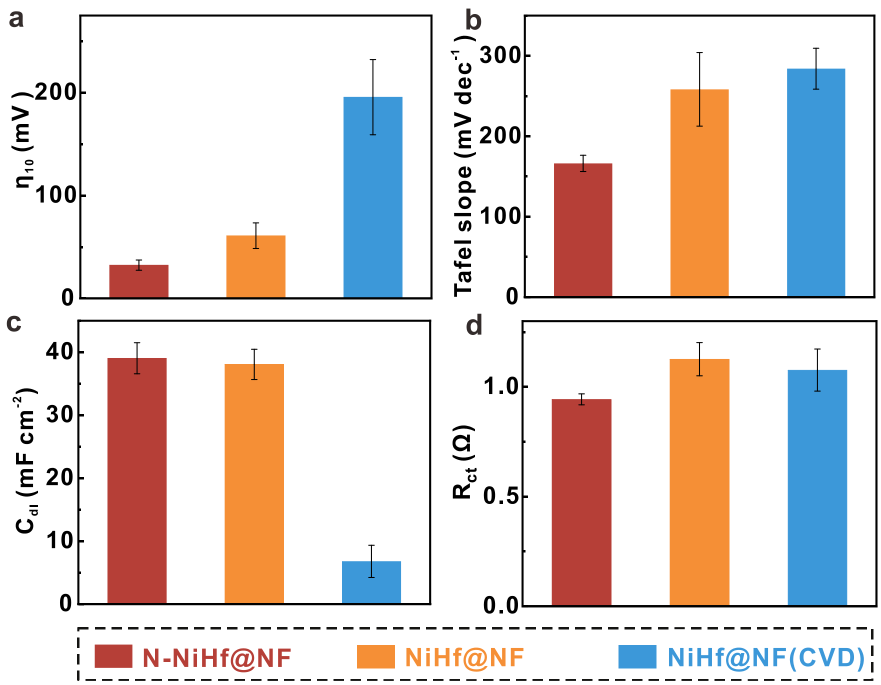

Figure S9. Repeatability data and standard error bars in 1.0 M KOH.

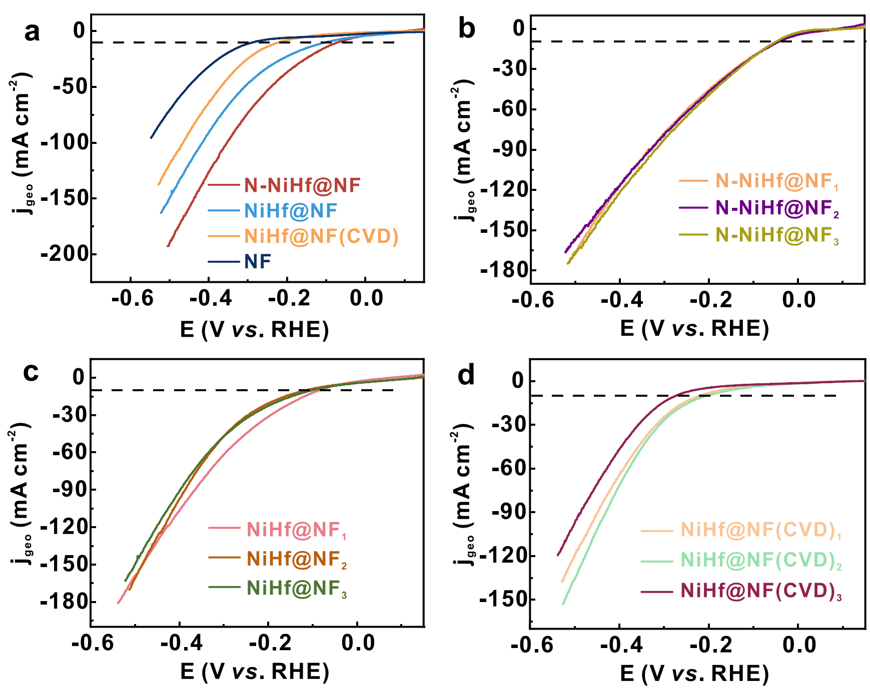

Figure S10. The HER activity of N-NiHf@NF, NiHf@NF, NiHf@NF(CVD), blank NF in 1.0 M KOH+0.5 M NaCl electrolyte. (a) LSV curves. Repetitive data of (b) N-NiHf@NF, (c) NiHf@NF, and (d) NiHf@NF(CVD).

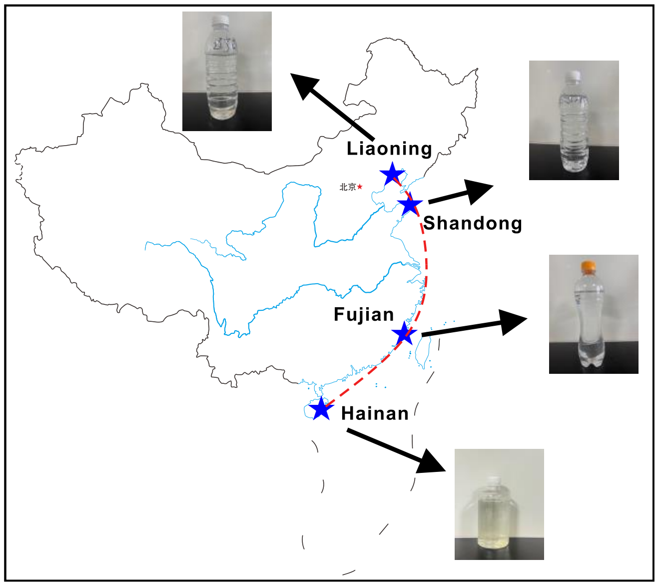

Figure S11. Photographs of seawater collected in different parts of China.

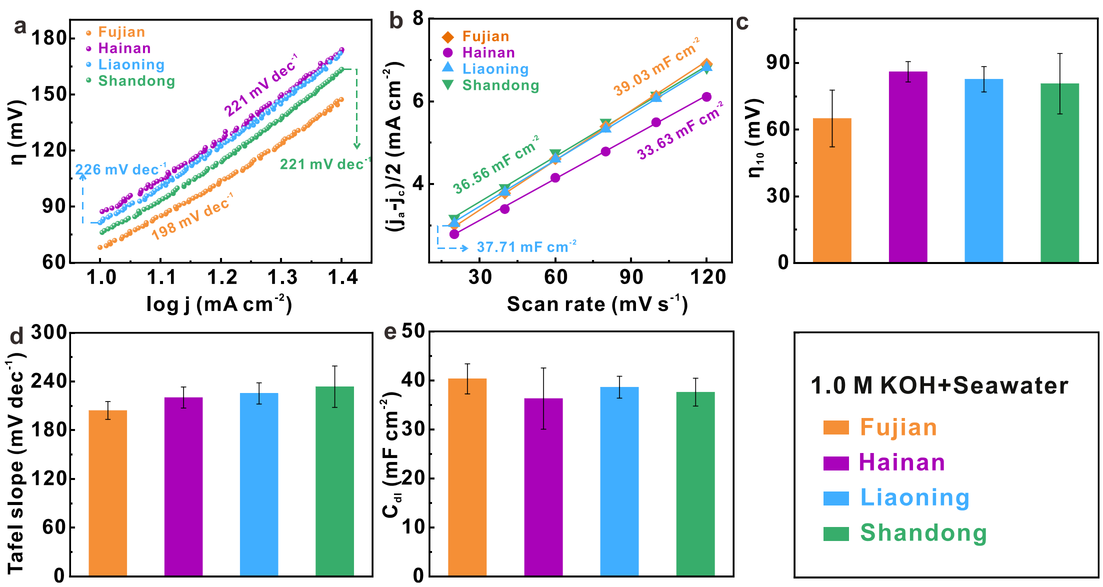

Figure S12. N-NiHf@NF in 1.0 M KOH+Seawater of electrochemical properties. (a) Tafel slope, (b) C_{dl}, and (c-e) repeatability of performance indicators.

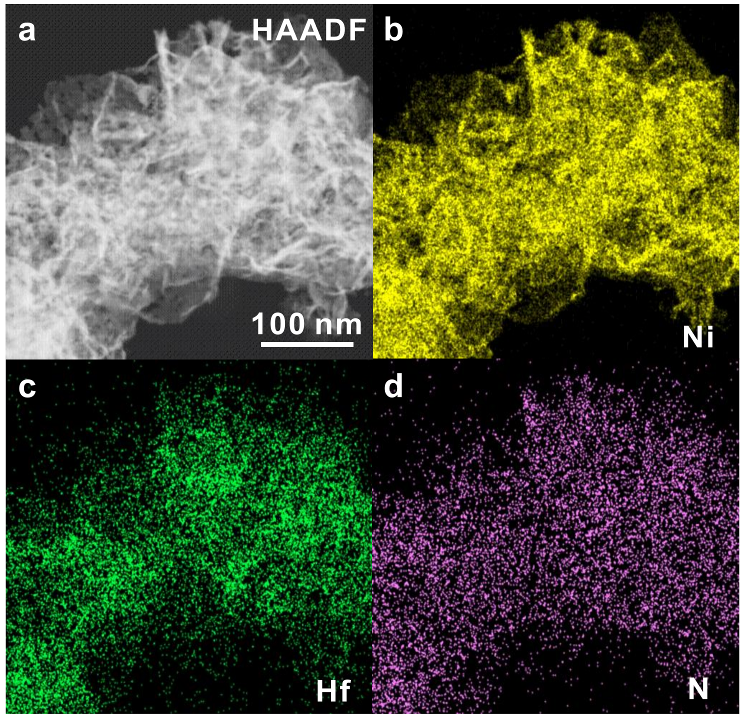

Figure S13. HAADF-STEM image and corresponding elemental mappings of N-NiHf@NF.

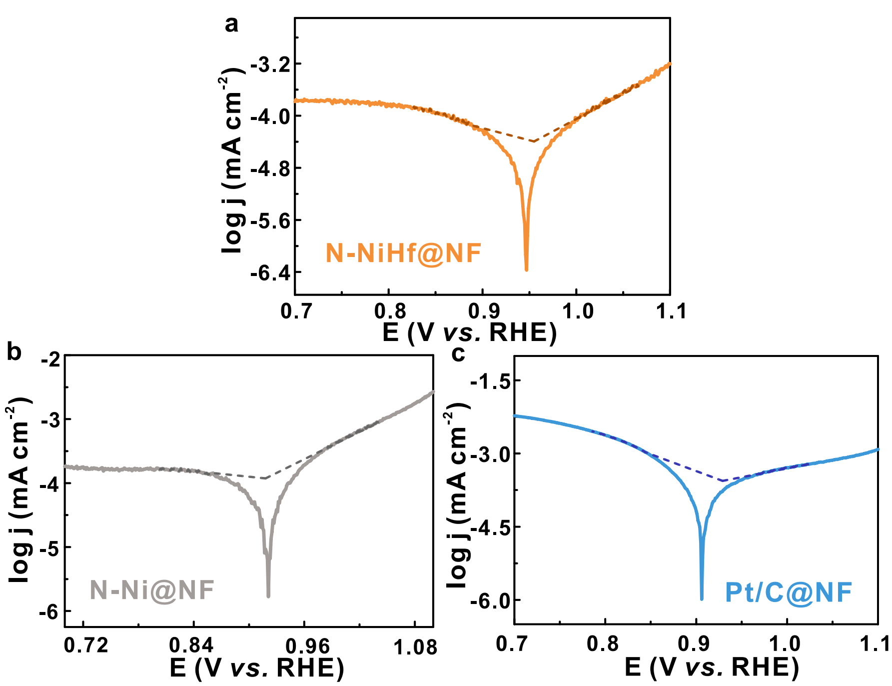

Figure S14. Corrosion polarization curves of (a) N-NiHf@NF (b) N-Ni@NF (c) Pt/C@NF.

Table S1. Fitting parameters of N-NiHf@NF catalyst under EXAFS spectra (C.N: coordination number; R: bond distance; E_0: energy shift; R factor: goodness or fit).

Catalyst	Edge	Path	C.N	R(Å)	E_0(eV)	R factor
N-NiHf@NF	Ni	Ni-Ni	4.93±0.92	2.48	-8.243	0.019
	Hf	Hf-N	10.75±2.75	2.05	-8.028	0.0089
Ni foil	Ni	Ni-Ni	11.99±0.26	2.45	-5.11	0.0054
NiO	Ni	Ni-O	5.94±0.018	2.17	-7.81	0.0019
		Ni-Ni	11.79±0.74	2.87		
HfO_2	Hf	Hf-O	8.0±0.5914	2.112	8.452	0.026

$S0^2$ was fixed as 0.85. Data ranges: $3 < k < 11$ Å^{-1}, $1 < R < 3$ Å. The number of variable parameters is 5. out of a total of 13.7 independent data points. N is the coordination number. R is the distance between absorber and backscatter atoms. σ^2 is the Debye-Waller factor. R-factor is residual factor.

Table S2. EIS fitting parameters of catalysts in 1.0 M KOH.

Electrodes / Parameter	N-NiHf@NF	NiHf@NF	NiHf@NF(CVD)	NF
R_{ct} (Ω)	0.944	1.165	1.185	1.415
R_s (Ω)	0.57	0.58	0.68	0.59

Table S3. Comparison of HER performance of N-NiHf@NF nanoalloy and reported alloy catalysts in 1.0 M KOH electrolyte.

Electrodes	**η_{10} (mV)**	**Tafel slope (mV dec^{-1})**	**Ref.**
N-NiHf@NF	**30**	**157**	**This work**
NiCoCu-$Mo_{0.078}$	35	50.12	[S4]
$Cu_{50}Mo_{50}$ alloy	22	40	[S5]
FeCoMo@NG-P	101	101	[S6]
RuNi-alloy@SC	50.5	65.52	[S7]
d-TiCuRu	40.5	40	[S8]
FeCoNi alloy	52	60	[S9]
Ni-Co alloy	54	30	[S10]
RuIr@BCN	28	39	[S11]

Table S4. EIS fitting parameters for N-NiHf@NF in different electrolyte.

electrolyte / Parameter	**1 M KOH**	**1.0 M KOH + 0.5 M NaCl**	**1.0 M KOH + Seawater**
R_{ct} (Ω)	0.944	1.231	1.028
R_s (Ω)	0.57	0.57	0.48

Table S5. Comparison of HER performance of N-NiHf@NF at different seawater.

Electrolyte	η_{10} (mV)	Tafel slope (mV dec^{-1})	C_{dl} (mF cm^{-2})
1 M KOH+Seawater (Fujian)	68	198	39.03
1 M KOH+Seawater (Hainan)	87	221	33.63
1 M KOH+Seawater (Liaoning)	81	226	37.71
1 M KOH+Seawater (Shandong)	76	221	36.65

Table S6. Comparison of HER performance of N-NiHf@NF nanoalloy and reported alloy catalysts in alkaline seawater electrolyte.

Electrodes	Electrolyte	η_{10} (mV)	Tafel slope (mV dec^{-1})	Ref.
N-NiHf@NF	1 M KOH+Seawater	68	198	This work
RuIr alloy	1 M KOH+Seawater	75	51.2	[S12]
Pt-NiCu alloy	Seawater	267	144	[S13]
FeRu/MoO_2@Mo	1 M KOH+Seawater	65	/	[S14]
RuMo/Cu_2O@C	1 M KOH+Seawater	24	49.9	[S15]
Co@RuCo	1 M KOH+Seawater	59	/	[S16]
CoMoP@C	Seawater	450	530	[S17]

FeCoNiMnRu	1 M KOH+Seawater	35	41	[S18]
FeCoNi	1 M KOH+Seawater	150	233	[S18]
Co/C-N	1 M KOH+Seawater	250	/	[S19]
Ni_2P-Fe_2P/NF	1 M KOH+Seawater	135	86	[S20]
NiRuIrG	1 M KOH+Seawater	200	48	[S21]
Ni-N_3	1 M KOH+Seawater	139	120	[S22]

Table S7. Quantitative XPS analysis before and after electrochemical stability measurement of N-NiHf@NF electrode.

Elements	**Atomic (%)**		**Mass (%)**	
	Before	After	Before	After
Ni 2p	28.94	9.28	20.1	5.63
Hf 4f	1.81	1.32	3.24	1.53
N 1s	4.85	1.67	8.95	2.00

Reference

[S1] Ravel B, Newville M. ATHENA, ARTEMIS, HEPHAESTUS: data analysis for X-ray absorption spectroscopy using IFEFFIT. *Synchrotron Radiation*, 2005, 12, 4, 537-541.

[S2] Shao L, Han X, Shi L, et al. *In situ* generation of molybdate-modulated nickel-iron oxide electrodes with high corrosion resistance for efficient seawater electrolysis. *Advanced Energy Materials*, 2024, 14, 4, 2303261.

[S3] Kang X, Yang F, Zhang Z, et al. A corrosion-resistant RuMoNi catalyst for efficient and long-lasting seawater oxidation and anion exchange membrane electrolyzer. *Nature Communications*, 2023, 14, 1, 3607.

[S4] Qian G, Wang Y, Li L, et al. Strategies for tuning tensile strain and localized electrons in a Mo-doped NiCoCu alloy for enhancing ampere-level current density HER performance. *Advanced Functional Materials*, 2024, 34, 40, 2404055.

[S5] Chen L, Jian X, Gao Q, et al. Towards robust hydrogen evolution electrocatalysts in immiscible copper-molybdenum alloys by amorphization. *Journal of Materials Chemistry A*, 2025. 13, 12523-12533

[S6] Huang L, Li W, Shen X, et al. Phosphorus-bridged ternary metal alloy encapsulated in few-layered nitrogen-doped graphene for highly efficient electrocatalytic hydrogen evolution. *Journal of Materials Chemistry A*, 2022, 10, 13, 7111-7121.

[S7] Bai X, Pang Q Q, Du X, et al. Integrating RuNi alloy in S-doped defective carbon for efficient hydrogen evolution in both acidic and alkaline media. *Chemical Engineering Journal*, 2021, 417, 129319.

[S8] Tian J, Hu Y, Lu W, et al. Dealloying of an amorphous TiCuRu alloy results in a nanostructured electrocatalyst for hydrogen evolution reaction. *Carbon Energy*, 2023, 5, 8, e322.

[S9] Yang Y, Lin Z, Gao S, et al. Tuning electronic structures of nonprecious ternary alloys encapsulated in graphene layers for optimizing overall water splitting activity. *ACS Catalysis*, 2017, 7, 1, 469-479.

[S10] Wang J, Shao H, Ren S, et al. Fabrication of porous Ni-Co catalytic electrode with high performance in hydrogen evolution reaction. *Applied Surface Science*, 2021, 539, 148045.

[S11] Qiu T, Cheng J, Liang Z, et al. Unveiling the nanoalloying modulation on hydrogen evolution activity of ruthenium-based electrocatalysts encapsulated by B/N co-doped graphitic nanotubes. *Applied Catalysis B: Environmental*, 2022, 316, 121626.

[S12] Yu Y, Xu H, Xiong X, et al. Ultra-thin RuIr alloy as durable electrocatalyst for seawater hydrogen evolution reaction. *Small*, 2024, 20, 46, 2405784.

[S13] Yi L, Chen X, Wen Y, et al. Solidophobic surface for electrochemical extraction of high-valued $Mg(OH)_2$ coupled with H_2 production from seawater. *Nano Letters*, 2024, 24, 19, 5920-5928.

[S14] Huo M, Sun X, Sun J, et al. High-performance FeRu alloy electrocatalyst integrated with a Mo substrate for hydrogen evolution reaction in seawater. *Small*, 2025, 2412729.

[S15] Yang X, Shen H, Xiao X, et al. Regulating interfacial H_2O activity and H_2 bubbles by core/shell nanoarrays for 800 h stable alkaline seawater electrolysis. *Advanced Materials*, 2025, 2416658.

[S16] Huang H, Jung H, Park C Y, et al. Surface conversion derived core-shell nanostructures of Co particles@RuCo alloy for superior hydrogen evolution in alkali and seawater. *Applied Catalysis B: Environmental*, 2022, 315, 121554.

[S17] Ma Y, Wu C, Feng X, et al. Highly efficient hydrogen evolution from seawater by a low-cost and stable CoMoP@C electrocatalyst superior to Pt/C. *Energy & Environmental Science*, 2017, 10, 3, 788-798.

[S18] Liu G, Song C, Li X, et al. Defect-rich FeCoNiMnRu high-entropy alloys with activated interfacial water for boosting alkaline water/seawater hydrogen evolution. *Chemical Engineering Journal,* 2025, 509, 161070.

[S19] Gao S, Li G, Liu Y, et al. Electrocatalytic H_2 production from seawater over Co, N-codoped nanocarbons. *Nanoscale,* 2015, 7, 6, 2306-2316.

[S20] Wu L, Yu L, Zhang F, et al. Heterogeneous bimetallic phosphide Ni_2P-Fe_2P as an efficient bifunctional catalyst for water/seawater splitting. *Advanced Functional Materials,* 2020, 31, 2006484.

[S21] Maria S, Eleonora P, Davide S. Active and stable graphene supporting trimetallic alloy-based electrocatalyst for hydrogen evolution by seawater splitting. *Electrochemistry Communications,* 2020, 111, 106647.

[S22] Zang W, Sun T, Yang T, et al. Efficient hydrogen evolution of oxidized Ni-N_3 defective sites for alkaline freshwater and seawater electrolysis. *Advanced Materials,* 2021, 33, 2003846.